Journal of New Technology and Materials
JNTM
Vol. 05, N°02 (2015)08-19

OEB Univ. Publish. Co.

Thermal Analysis of Partially Stabilized Zirconia and Lanthanum Magnesium Hexaaluminate as Thermal Barrier Coatings over Hastelloy X Gas Turbine Blade

A. K. Saini[a] and Nikhil Shandil[b]

[a,b]*Department of Mechanical Engineering, UIET, Panjab University SSG Regional Centre, Hoshiarpur 146021 (Punjab), India*

[a,*]*Email: ajay_9avd@yahoo.co.in*

Received date: July 02, 2015; accepted date: October 03, 2015

Abstract

The sprayed partially stabilized zirconia (8 % by wt. yttria) and lanthanum magnesium hexaaluminate were investigated as materials for thermal barrier coatings over Hastelloy X as substrate for a high temperature gas turbine blade model using NiCrAlY as an interlayer bond coat material. The temperature and heat flux based steady and transient thermal analyses were performed over variable thickness models for two different coating materials using a FEM based commercial ANSYS Workbench v14.5 software package. It was found that under applied thermal loading conditions, just a 200 microns thick zirconia coating used with 150 microns NiCrAlY layer was capable to reduce steady state substrate temperatures by 35.6 % and proved to be 3.72 % more effective than an equal thickness lanthanum magnesium hexaaluminate coating. Similarly, steady state top surface heat flux was found to be 15.7 % lesser for the former as compared to later. The increased thickness of coatings observed further reductions in the substrate temperatures and top surface heat flux values, however, the zirconia coatings were found to be more effective than lanthanum aluminate coatings at higher thicknesses in terms of suppressions of heat penetration and substrate temperatures. A steady state top coat – bond coat interface heat flux analysis further helped in anticipating that thin films of zirconia could be more durable than lanthanum aluminate coatings in the high flux working conditions as prevailing inside a gas turbine system.

Keywords: *Thermal barrier coating (TBC); Partially stabilized zirconia; Lanthanum magnesium hexaaluminate; Gas turbine; Hastelloy X*

1. INTRODUCTION

Over the years in the history of gas turbines, technological advancements led efforts have been made to increase efficiency of the system. These efforts have ultimately made it possible to achieve turbine inlet temperature (TIT) of 1600 °C and over in the modern advanced gas turbine systems as compared to 800 °C during 1960s [1-2]. However, such elevated TITs being high above even melting point of the blade material demand for high cooling loads for the blades and advanced/sophisticated cooling techniques [3]. Due to this, high temperature materials have always been a focus of attention for the metallurgical scientists and researchers. In fact, improvements in TITs have been possible with the improvements in the field of high temperature creep resistant blade materials from conventionally cast polycrystalline to directional solidified and to single crystal materials till 2000 and then to superalloys of Ni and Cr [4-5]. As a parallel area of research, thermal barrier coatings (TBCs) have also been active in this regard [6]. These coatings are of low thermal conductivity ceramic materials which act as insulating barrier to the substrate material in the high flux working atmosphere and can be put over the metallic substrate surface using various techniques like atmospheric plasma spray (APS), chemical vapor deposition (CVD), high velocity oxy fuel (HVOF), electron beam spray (EBS) etc., using an intermediate bond coat layer of suitable material, which not only increases adherence of TBC to the substrate, but also

prevents oxidation of the later and compensates for the mismatch of thermal coefficients of expansion between the two [7-8].

In the present work, two different ceramic materials, one being zirconia (ZrO_2) partially stabilized with yttria (Y_2O_3) and another being lanthanum magnesium hexaaluminate ($LaMgAl_{11}O_{19}$) were investigated as TBC materials for a gas turbine blade model made up of Hastelloy X using a popular FEM based commercial ANSYS Workbench v14.5 software package. The temperature and heat flux analysis were carried out for steady state as well as transient state heat transfers for different thicknesses of the coatings so as to investigate their effect in reducing substrate temperatures and also to anticipate a durability comparison between them in high temperature environments.

2. MATERIALS

2.1. Blade substrate

A nickel base superalloy named Hastelloy X was selected as the substrate material for gas turbine blades, which is basically an alloy of nickel and chromium (Ni-47%, Cr-22%, Fe-18%, Mo-9%, Co-1.5%, W-0.6%) possessing high resistance to oxidizing atmosphere, excellent forming and welding characteristics and good workability. As per Haynes International High-Temperature Alloys, HASTELLOY® X undergoes a per side metal loss of only 1.5 mils (0.0381 mm) excluding Continuous Internal Penetration (CIP), when exposed to an oxidizing atmosphere at 1095 ºC for 1008 hours cyclically brought down to room temperature once a week. Moreover, total metal affected per side for the same alloy exposed to a hot corrosive environment of combustion products of a fuel oil (containing 0.4 % sulfur and 5 ppm of sea salt) at a flow velocity of 4 m/s, temperature of 900 ºC, test period of 1000 hours and thermal loading applied cyclically each hour, is only 6.8 mils (0.173 mm). Table I gives some other thermo-physical properties of HASTELLOY® X as mentioned by Haynes International High-Temperature Alloys.

Property	Value
Density (kg/m^3) at 22 ºC	8220
Poisson's ratio at 22 ºC	0.320
Melting temperature (ºC)	1260-1355
Thermal conductivity (W/m K) at 927 ºC	27.2
Specific heat (J/kg K) at 1093 ºC	858
Coefficient of thermal expansion (ºC^{-1}) in the range of 25-700 ºC	15.6 x 10^{-6}

Table I Properties of HASTELLOY® X alloy

2.2. Bond Coat and Top Coat Materials

Two different sprayed materials, namely partially stabilized zirconia (ZrO_2) with 8% wt. Y_2O_3 (so designated as 8Y-PSZ) and lanthanum magnesium hexaaluminate ($LaMgAl_{11}O_{19}$) were selected as the materials for thermal barrier coatings applied over the gas turbine blade substrate of Hastelloy X through an intermediate layer of bond coat of NiCrAlY. These materials 8Y-PSZ (melting temperature 2600 ºC) and lanthanum magnesium hexaaluminate (melting temperature 2080 ºC) were selected as the TBC top layer materials for the analysis because of their low thermal conductivity value and their compatibility with bond coat. Various thermal properties of sprayed NiCrAlY, 8Y-PSZ and Lanthanum magnesium hexaaluminate (LA) as used in this investigation are given in Table II [9-11].

Property	8Y-PSZ	LA	NiCrAlY
Thermal conductivity (W/m K)	1.0	2.2	11.6
Coefficient of thermal expansion (ºC^{-1})	10 x 10^{-6}	10.7 x 10^{-6}	12 x 10^{-6}
Specific heat (J/kg K)	500	900	500

Table II Thermal properties of sprayed/coated materials

3. MODELING AND ANALYSIS

A typical gas turbine blade of height 75 mm was modeled by using Pro E v5.0 as geometric modeling tool. A total of eleven such models were created to do thermal analysis for one uncoated blade and ten coated blades for 8Y-PSZ and lanthanum magnesium hexaaluminate in five different TBC thicknesses as mentioned in Table III. Further, all the models were kept to be dimensionally same and NiCrAlY was used as the bond coat interlayer in all ten coated models.

Model designation	Specifications	
	Bond coat material (thickness in microns)	Top coat material (thickness in microns)
0/0	–	–
150/200 PSZ	NiCrAlY (150)	8Y-PSZ (200)
150/200 LA	NiCrAlY (150)	LA (200)
200/400 PSZ	NiCrAlY (200)	8Y-PSZ (400)
200/400 LA	NiCrAlY (200)	LA (400)
250/600 PSZ	NiCrAlY (250)	8Y-PSZ (600)
250/600 LA	NiCrAlY (250)	LA (600)
300/800 PSZ	NiCrAlY (300)	8Y-PSZ (800)
300/800 LA	NiCrAlY (300)	LA (800)
350/1000 PSZ	NiCrAlY (350)	8Y-PSZ (1000)
350/1000 LA	NiCrAlY (350)	LA (1000)

Table III Models formed for thermal analysis

Fig. 1 shows a typical model of gas turbine blade used in this analysis with TBC set up employed over it while cross sectional details of the blade are shown in Fig. 2.

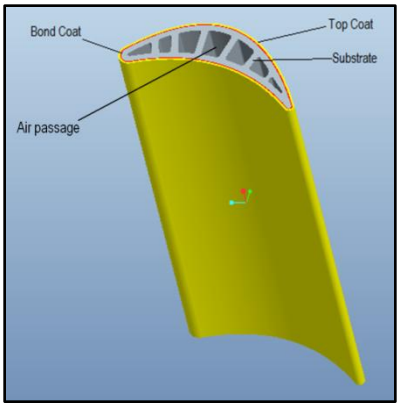

Fig. 1. Gas turbine blade model

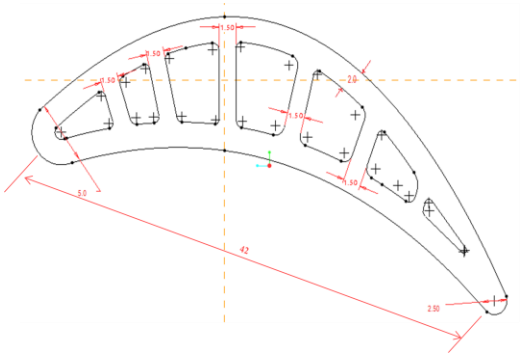

Fig. 2. Cross section of blade model

ANSYS workbench v14.5 commercial analysis package was used for steady state and transient state analysis of various coated and uncoated models. The convective thermal conditions of 1800 K with a convective coefficient of 1681 W/m^2 K were used for the hot gases flowing over the blade. Similarly, cooling of the blade was simulated with convective conditions of 300 K (assumed intercooled) and a film coefficient of 203 W/m^2 K for coolant air passing through the air passages. These particular heat transfer coefficient values were considered from the approximate calculations since objective of this paper was to establish a comparative effect of investigated TBC materials. Further, convection coefficient for coolant air was kept low to illustrate the significance of cooling in gas turbine blades as temperatures within the blade go very high beyond the limiting value under this insufficient cooling and effect of TBC is highly significant in this regard.

Under Steady-State Thermal and Transient Thermal analysis systems of ANSYS, program controlled meshing was done for the models as shown in Fig. 3

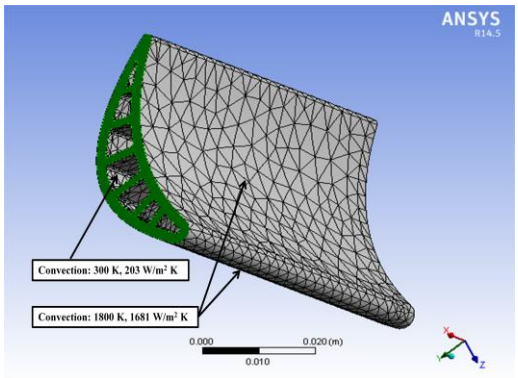

Fig. 3. Meshed blade model with applied thermal loading

4. RESULTS AND DISCUSSION

Simulations were performed over ANSYS workbench v14.5 as analysis module for all different models of coated and uncoated blades by taking thermal loading conditions as mentioned earlier. All the models were solved under steady state thermal and transient thermal analysis systems for temperature as well as heat flux values. Further, the thermal analysis for temperatures was done for the complete coated models, only substrate parts of the models, top surface of the top coat and that of substrate. Similarly heat flux variations were found for the complete coated models, only substrate parts of the models, top surface of top coat, bottom surface of top coat and top surface of bond coat.

4.1. Temperature Analysis

While analyzing steady state temperature results of various selected models for a particular top coat material, it was observed that the temperature maxima for the complete substrate material and substrate surface were exactly same for all the models. Similarly, temperature maxima for the complete coated models and their corresponding top ceramic surfaces were also found to be alike. This is an obvious observation otherwise also since heat penetrates within the turbine blade from surrounding working atmosphere of hot gases. Fig. 4 shows steady state temperature variation for substrate surface (top surface) of uncoated (0/0) model. The effects of 8Y-PSZ/NiCrAlY TBC on the steady state temperature variations over substrate top surface and top surface of each coating model are shown in Fig. 5 and Fig. 6, respectively. Similarly, steady state temperature variations at the substrate top surface and TBC top surface for different thickness models of LA/NiCrAlY TBC are shown in Fig. 7 and Fig. 8, respectively.

The results found in steady state thermal analysis under ANSYS were compared for all the models to observe the effect of thermal barrier coating over gas turbine blade and to realize the effect of thickness of TBC in performance of system.

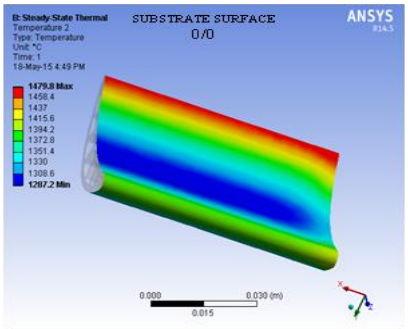

Fig. 4. Steady state temperature variation over substrate surface of uncoated model

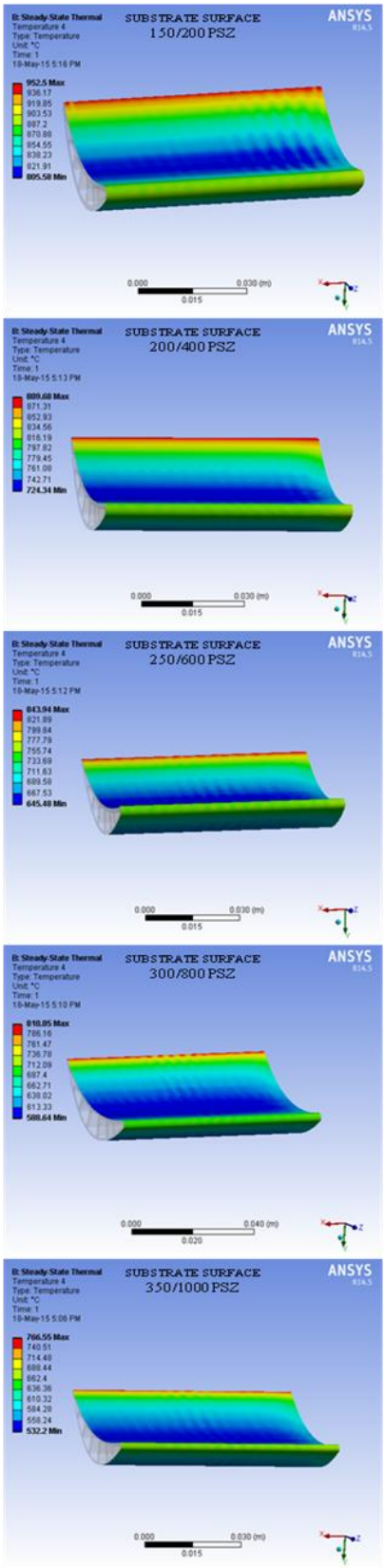

Fig. 5. Steady state temperature variation over substrate surface for 8Y-PSZ/NiCrAlY coated models

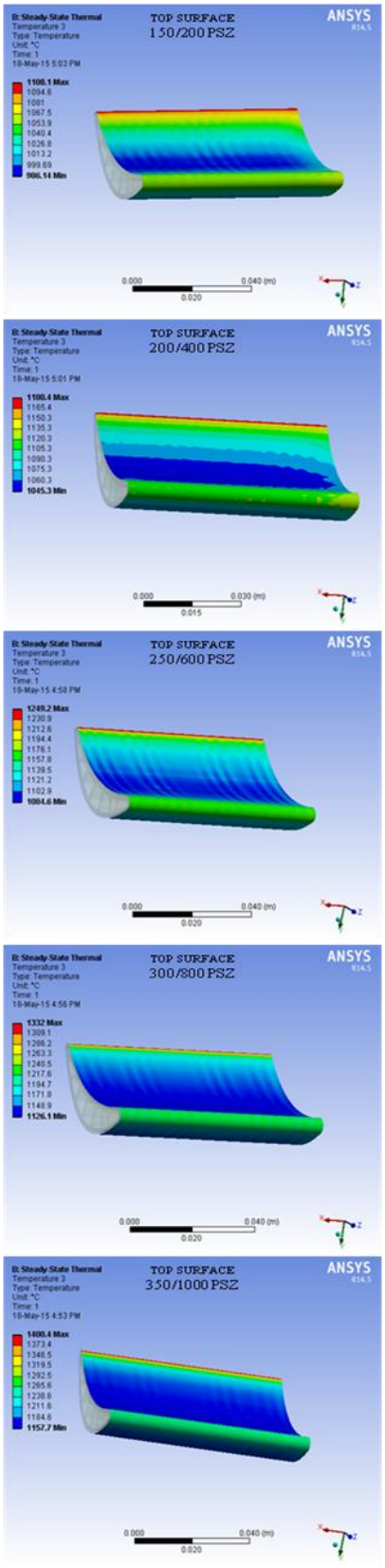

Fig. 6. Steady state temperature variation over top surface for 8Y-PSZ/NiCrAlY coated models

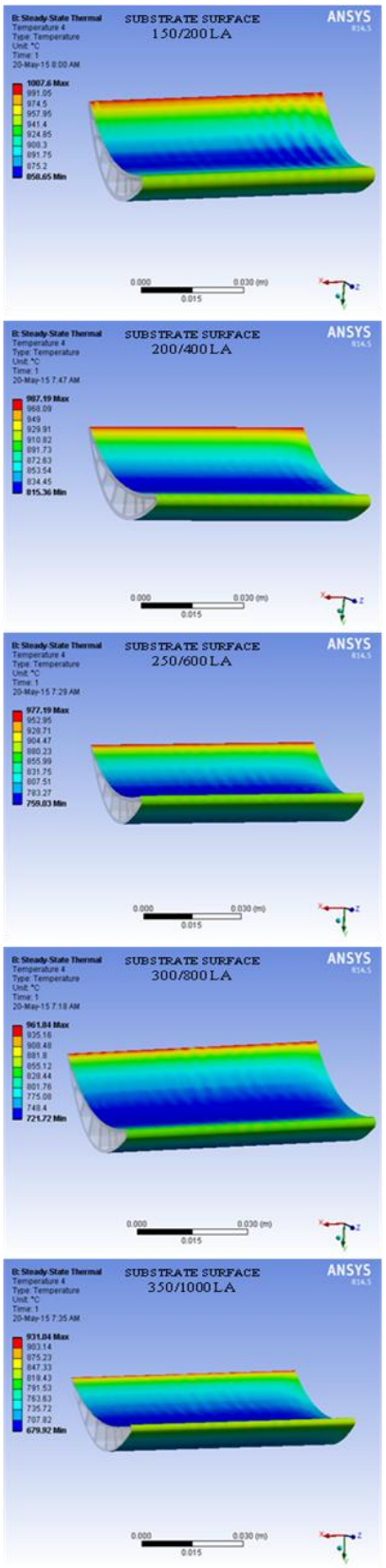

Fig. 7. Steady state temperature variation over substrate surface for LA/NiCrAlY coated models

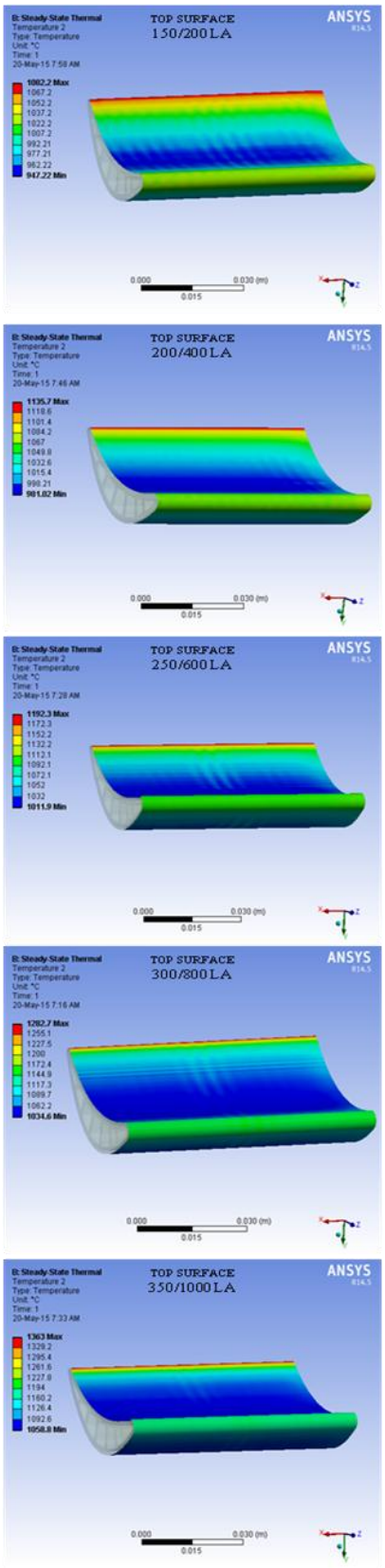

Fig. 8. Steady state temperature variation over top surface for LA/NiCrAlY coated models

The comparative results for different thickness models for 8Y-PSZ and LA coatings have been shown in Fig. 9. The comparison has been carried out with reference to the maximum temperature prevailing at the substrate surface of model and its top surface at steady state conditions. It is clear from both the figures that as compared to the uncoated blade model (0/0), TBC coated models experience lesser temperatures at substrate surface. Also, as the coating thickness increases from 150/200 model to 350/1000 model, the maximum temperature of top ceramic coat surface also goes on increasing for both types of coatings. This data is supporting to the statement that thermal barrier coating helps in reducing substrate temperatures by acting as a resistance to heat penetration and by retaining maximum of the heat of the surrounding working fluid of the high temperature thermal system within fluid itself.

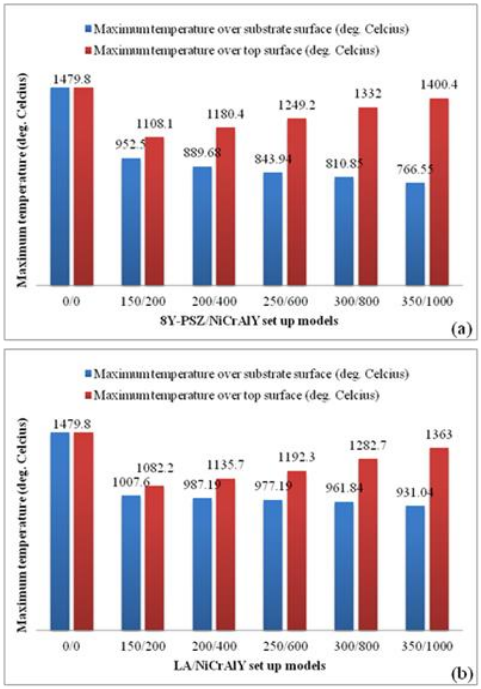

Fig. 9. Steady state maximum temperature over substrate surface and top surface (a) 8Y-PSZ/NiCrAlY coated models and, (b) LA/NiCrAlY coated models

The increase in thickness of coating significantly decreases temperatures of the substrate surface. A 150/200 PSZ model coating is sufficient enough to lower down maximum temperature of the substrate surface from 1479.8 °C to 952.5 °C, giving thereby a decrease of 35.63 %. It is worth noting here that taking into account the melting temperature of Hastelloy-X, temperature of 1479.8 °C is undesirable at all as compared to 952.5 °C. Similarly, 350/1000 PSZ model coating has the potential to reduce substrate

temperature by 48.5 %. In case of 150/200 LA model, substrate surface maximum temperature was found to be 31.91 % less than uncoated model. This effect of thickness of PSZ and LA coatings in decreasing maximum temperature of gas turbine blade material has been plotted in Fig. 10, which shows that 8Y-PSZ/NiCrAlY TBC is more effective than LA/NiCrAlY coating in lowering substrate temperatures. Moreover, a thicker 8Y-PSZ coating behaves still more effectively in this regard than a similar thickness LA/NiCrAlY coating.

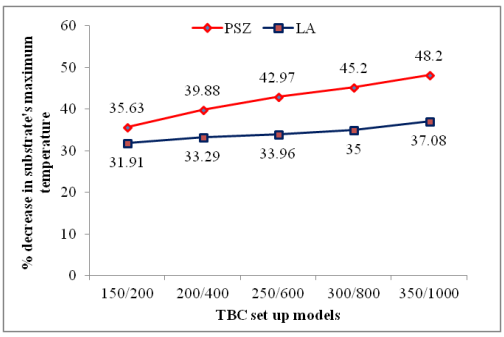

Fig. 10. Effect of TBC thickness in reducing substrate's maximum temperature

Under transient thermal analysis system, all the models were solved for an exposure time of 10 seconds to the applied thermal loading conditions. The results of analysis for 8Y-PSZ/NiCrAlY and LA/NiCrAlY coatings are plotted in Fig. 11 and Fig. 12. Fig. 11 gives time-wise variation in the maximum temperature built up over the substrate surface of each coated model as compared to that in case of uncoated model for both types of coatings. It is clear that temperature at the substrate surface grows at a very fast rate in case of 0/0 (uncoated) model in comparison to all coated models of PSZ or LA. As the coating thickness increases, falling slopes of the transient curves indicate that the temperature maxima over the substrate surface goes on decreasing. This clearly supports that a higher thickness TBC set up applied over the base material has a higher potential of decreasing temperatures of the later. Moreover, lower slopes of the transient curves in case of PSZ coated models as compared to LA coated models as observed in 10 seconds transient analysis, indicate that PSZ coatings serve more effectively than the later ones. It is further observable from the temperature curves for both types of coatings that 150/200 TBC coating set up causes a high temperature suppression within the substrate material, which is even higher than that caused by 350/1000 coating set up over 150/200 one. This particular result is useful in context with the fact that as coating thickness increases, its material as well as spray costs do also increase significantly with decrease in the life of coating in its high temperature working atmosphere.

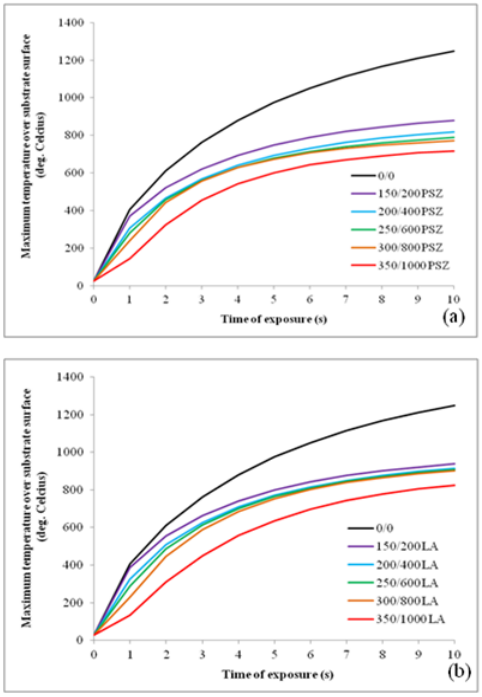

Fig. 11. Transient variation of maximum temperature over substrate surface (a) 8Y-PSZ/NiCrAlY coated models and, (b) LA/NiCrAlY coated models

To visualize the performance of TBC over substrate, growth of maximum temperature over top TBC surface of each coated model for both types of coatings was also plotted against time of exposure and is shown in Fig. 12. It is clear from the figure that just during the earlier phase of exposure of the gas turbine blade to high temperature operating atmosphere of hot gases, thickest coating model of PSZ (350/1000 PSZ) experiences a very high maximum temperature over its top surface. This temperature maxima over the top surface of coating is lesser in case of thinner coating models and is minimum in case of uncoated 0/0 model. Also, in the succeeding phase of exposure to hot gases, slope of 150/200 PSZ coating model curve is significantly lesser than that of 0/0 model and slopes of transient curves can be clearly observed as decreasing with increase in thickness of TBC. This again means that the temperature growth over the top surface of coating in most of the exposure time period is lesser for thicker PSZ coating as compared to thinner one and the thicker coating has therefore more effect in resisting heat penetration into the substrate from surrounding hot media.

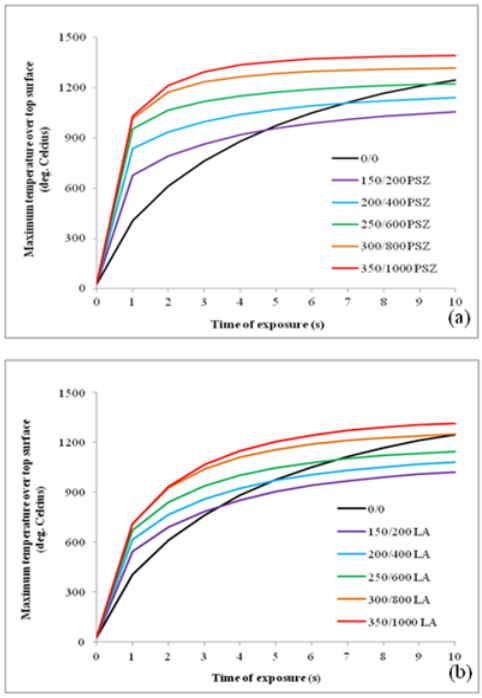

Fig. 12. Transient variation of maximum temperature over top TBC surface (a) 8Y-PSZ/NiCrAlY coated models and, (b) LA/NiCrAlY coated models

Similar observations can be made from transient curves of LA coating models of Fig. 12. However, it is here important to note that as compared to PSZ models, it takes longer for the top surface temperature maxima of LA coated models to settle down to a steady value. This again claims PSZ coatings as superior to LA coatings in reducing the heat penetrations. Further, it is again a general observation from transient curves for PSZ and LA coating models of Fig. 12 that effect of 200/400 LA over 150/200 LA is lesser than that of 200/400 PSZ over 150/200 PSZ. Same observation is also true for higher thickness models of PSZ and LA.

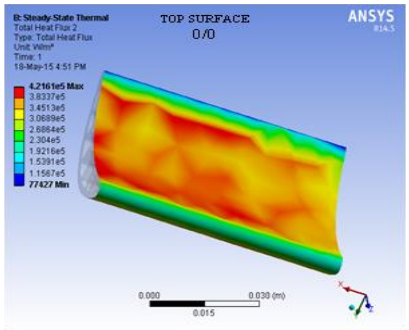

Fig. 13. Steady state heat flux variation over top surface for uncoated model

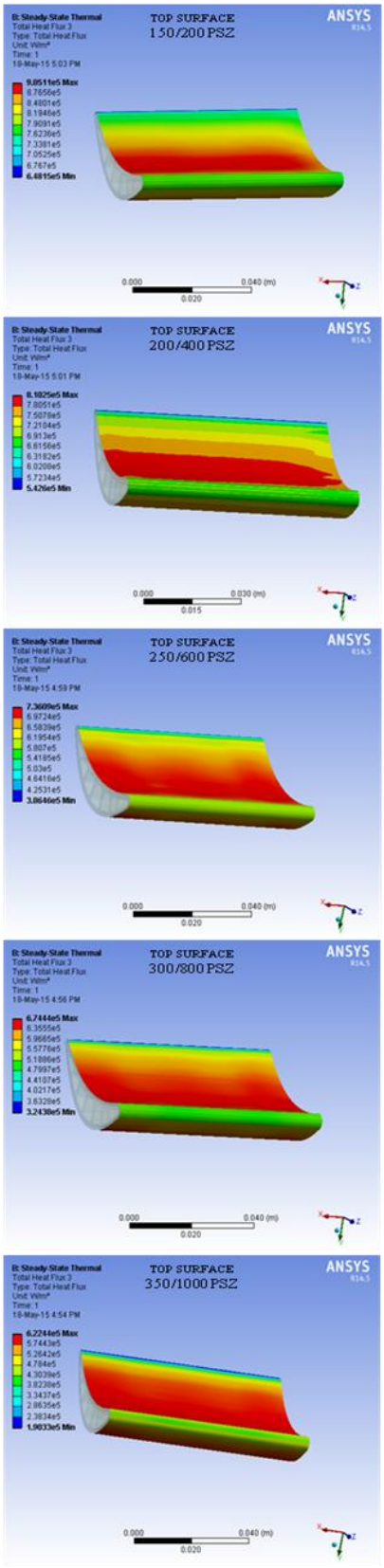

Fig. 14. Steady state heat flux variation over top surface for 8Y-PSZ/NiCrAlY coated models

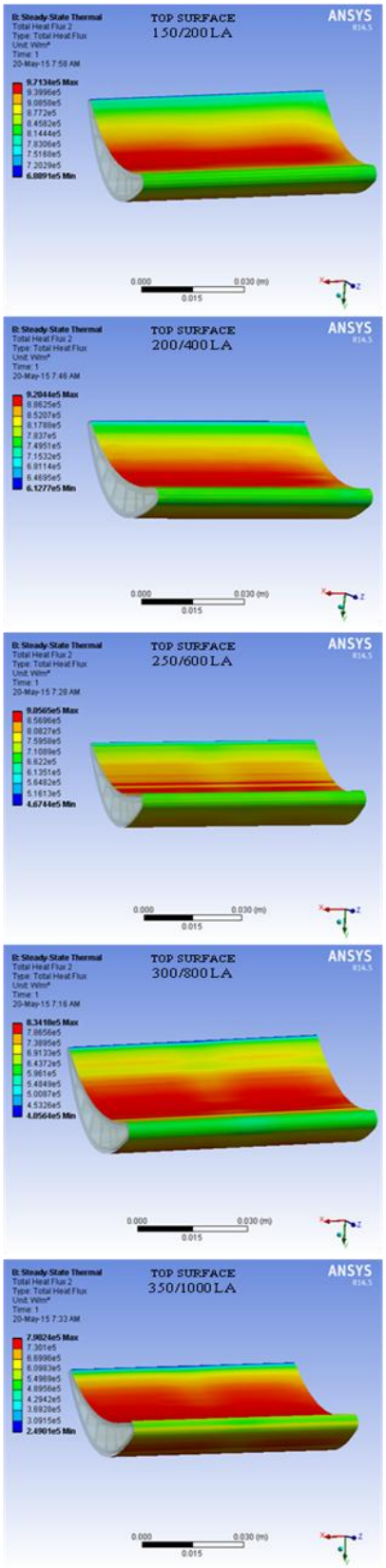

Fig. 15. Steady state heat flux variation over top surface for LA/NiCrAlY coated models

4.2. Heat Flux Analysis

Steady state heat flux variations for the top surfaces of uncoated model, 8Y-PSZ/NiCrAlY coated models and LA/NiCrAlY coated models as obtained from ANSYS investigation are shown in Fig. 13, Fig. 14 and Fig. 15, respectively. The figures show that value of maximum heat flux at the top surface of a TBC coated model exposed to hot environment is more than that in case of uncoated model. These results were used to compare different thickness coated models of two different types of TBCs and the illustration is shown in Fig. 16 for the percentage increase in maximum heat flux value at the top TBC surface of each coated model. As compared to a maximum thermal flux of 421.61 kW/m^2 for uncoated model, it is 905.11 kW/m^2 for 150/200 PSZ coated model and 971.34 kW/m^2 for 150/200 LA coated model, giving thereby hikes of 114.68 % and 130.39 % respectively. This huge rise in the heat flux at top surface is because of the fact that in case of TBC coated model, maximum temperature at the top surface is very lesser as compared to that in the uncoated case. Top surface maximum heat flux for LA coated models being more than PSZ models are further because of same reason that as compared to later, the former coated models experience lesser temperatures at their top TBC surfaces. But since increase in TBC thickness causes more and more temperatures over the top ceramic surface, so the temperature gap between hot media and top TBC surface goes on decreasing resulting into fall in heat flux value over the top surface. For the thickest PSZ model (350/1000 PSZ), top surface experiences a heat flux of 47.63 % higher than top surface of an uncoated model. While for the same thickness LA model, the value is 87.43 %. It is again significant here to conclude that higher thickness of TBC helps better in preventing heat loss from the working hot media into the coated material by reducing heat flux entering into the same. This effect of TBC may be taken in terms of improvement in the thermal efficiency of gas turbine system by increasing the turbine inlet temperature with/without reduced cooling loads. However, it is a clear observation from Fig. 16 that 8Y-PSZ/NiCrAlY TBC coatings have more potential to enhance thermal efficiency of the system than LA/NiCrAlY coatings and in particular, this potential gap between two different types of coatings increases with increase in thickness of coating.

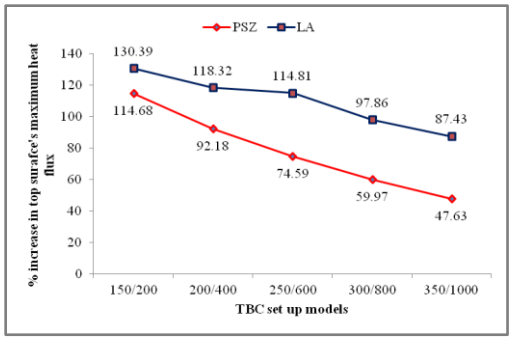

Fig. 16. Effect of TBC thickness over maximum heat flux at top surface

Transient state variation in the maximum heat flux was also plotted for a time period of 10 seconds for the top surface of each of the models and the graphs are shown in Fig. 17.

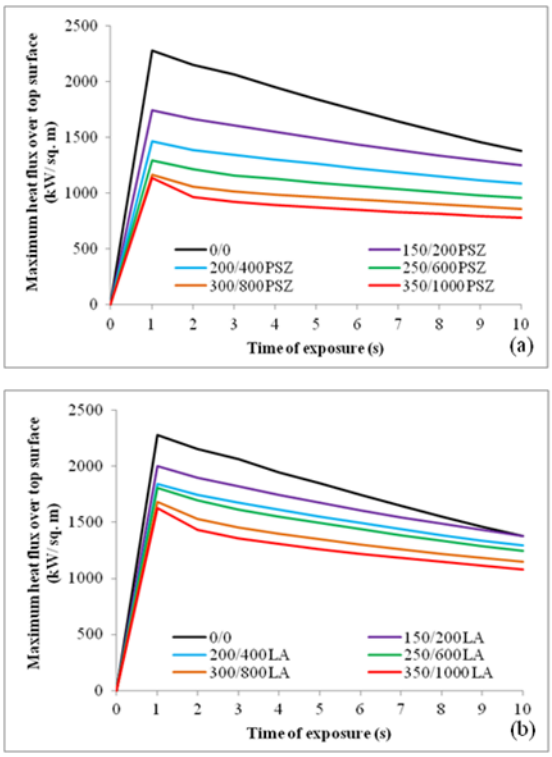

Fig. 17. Transient variation of maximum heat flux over top surface (a) 8Y-PSZ/NiCrAlY coated models and, (b) LA/NiCrAlY coated models

Fig. 17 shows that sudden exposure to the high temperature working atmosphere immediately throws a high heat flux over the exposed surface of the blade which further decreases with the passage of time till it would approach to steady conditions. However, uncoated blade model experiences highest thermal flux of 2280.2 kW/m^2 whereas peak flux value for 150/200 PSZ coated model is 1743.4 kW/m^2, causing thereby a decrease of 23.5 %. The thicker 8Y-PSZ coatings are further responsible for reducing this peak flux value by 35.8 %, 43.4 %, 48.9 % and 50.3 % for 200/400, 250/600, 300/800 and 350/1000 models, respectively. Similarly, as compared to the uncoated model, peak flux values at top surface of LA coated models are found to reduce by 12.0 %, 19.1 %, 20.7 %, 26.2 % and 28.6 % for 150/200, 200/400, 250/600, 300/800 and 350/1000 models, respectively. These data clearly highlight that a thicker TBC has higher potential of suppression of heat penetration than a thinner one, the effect being more for 8Y-PSZ coatings as compared to LA coatings.

4.3. Durability comparison

Although life of TBCs and their durability in high temperature working conditions depend upon many factors but here in this analysis focused upon temperatures and heat flux calculations, particularly interface between top coat (TC) and bond coat (BC) was investigated for both different types of coatings since generally this interface has been an initiative spot for TBC failures in many of the observations by the researchers worldwide [12-13]. The steady state heat flux variations for TC/BC interface were found for 8Y-PSZ/NiCrAlY as well as LA/NiCrAlY coated different thickness models using same previous analysis tool. The interface was considered both the ways as TC bottom surface and BC top surface, to find the flux mismatch and its pattern for various thickness models and the results are shown in Fig. 18.

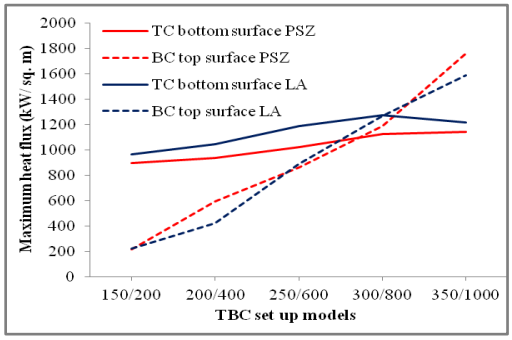

Fig. 18. Effect of TBC thickness over maximum heat flux at TC/BC interface

Basically heat flow rate should decrease within TC or BC with increase in coating thickness as it was also observed at the top surface for heat flux results. But Fig. 18 shows that interface heat flux here was rather found to increase from either side i.e. top coat side as well as bond coat side. It is because interface surface area associated with heat flux calculations goes on decreasing with increase in thickness of coating causing dominance over reduced heat flow rate with thickness increase. Further, rate of increase of heat flux is slower

for TC bottom surface than BC top surface for both types of coatings since top coat material is highly resistive (having very less thermal conductivity value) than bond coat material. However, when TBC thickness is very high, resistive effect of TBC material starts dominating over decrease in surface area and heat flux starts decreasing for TC bottom surface.

The results found above were used to calculate changes in maximum steady state heat flux values between TC bottom surface and BC top surface for different thickness models of both 8Y-PSZ/NiCrAlY and LA/NiCrAlY coatings. Fig. 19 shows variations in such flux mismatch values at TC/BC interface with thickness of each type of coating.

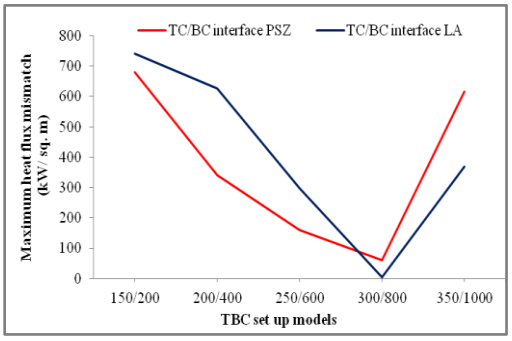

Fig. 19. Effect of TBC thickness over maximum heat flux at TC/BC interface

Fig. 19 shows that for the lower coating thicknesses (up to 250/600 model), 8Y-PSZ/NiCrAlY coatings experience less thermal flux mismatch at TC/BC interface than LA/NiCrAlY coatings. But this is reverse for higher thickness coatings. The mismatch was found to be minimum for 350/800 models with values of 60.6 kW/m^2 (for PSZ) and 5.1 kW/m^2 (for LA). It is further important here to establish that such interface thermal flux mismatch could be one of the factors leading to the observed TBC failure phenomena at TC/BC interface like cracks, delamination, spallation etc. Further, it can be concluded here that neglecting all other possible and established failure modes/causes of TBCs, 8Y-PSZ TBC coatings used with a bond coat of NiCrAlY are expected to serve longer at lower coating thicknesses while LA coatings might be lasting longer at higher coating thickness values. However as clear from Fig. 18 also, it is worth noting that at higher coating thicknesses, heat flux at the bond coat surface is getting very high and it even exceeds the flux value at the bottom surface of top TBC coat, which is undesirable since high heat flux at the bond coat may itself deteriorate it in due course of time. So as a whole, it is expected that 8Y-PSZ/NiCrAlY TBCs would be lasting a longer life while operating in high temperature applications of gas turbine as compared to the LA/NiCrAlY coatings.

5. CONCLUSION

Thermal barrier coatings of suitable materials applied over substrate materials working in the high temperature environments like gas turbines or diesel engines have high potential to lower the temperatures within substrates by providing thermal insulation to them and hence increase their service life also. Partially stabilized zirconia (8% by wt. yttria) and lanthanum magnesium hexaaluminate were investigated as such ceramic coatings using popular analysis software of ANSYS Workbench v14.5 over Hastelloy X as substrate material for a typical gas turbine blade model. An intermediate bond coat of NiCrAlY was used for both types of coatings. The analysis was carried out for variable coating thickness models in steady state as well as transient state modes using convection conditions of 1800 K, 1681 W/m^{2}K for hot gases and 300 K, 203 W/m^{2}K for coolant air. It was found that zirconia coatings suppressed the substrate temperatures to a greater extent than lanthanum aluminate coatings. Even a 200 microns top coat of the former with a 150 microns bond coat (referred as 150/200 PSZ model) was capable to lower steady state maximum temperature of substrate by 35.63 % against 31.91 % for the later (referred as 150/200 LA model). The increased thickness of coatings observed further reductions in the substrate temperatures. A 350/1000 PSZ model enhanced substrate temperature reductions to 12.57 % more than a 150/200 PSZ model against 5.17 % enhancement for similar thickness LA models. During heat flux analysis of various models of two different coatings, PSZ coatings were found to experience lesser heat flux at their top surfaces than equally thick LA coatings, meaning thereby that PSZ coatings are more effective in suppressing heat penetration within the material. Under steady state heat flux calculations, it was observed that top surface heat flux reductions for PSZ and LA coatings were improved respectively by 67.05 % and 42.96 % as the coating thickness increased from 150/200 to 350/1000. This again suggested that a particular increase in thickness makes PSZ coating more effective than LA coating. Further, a steady state maximum heat flux analysis was done for the bottom surface of top coat and top surface of bottom coat considering the importance of this interface in

governing life of TBCs in high flux atmospheres. It was anticipated that the deterioration at bond coat would likely be happening earlier in case of low thickness LA coatings and high thickness PSZ coatings due to a large mismatch in thermal flux values calculated from the two sides of interface. However, high thickness coatings (PSZ or LA) were individually found to experience high heat flux values at the interface, which itself might become a failure cause for any TBC. So, it was concluded that low thickness PSZ coatings would be better than LA coatings in all the aspects.

References

[1] T. Ai, J. Masada, E. Ito, *Mitsubishi Heavy Industries Technical Review* 51(1) (2014) 1−9

[2] P. Hancock, M. Malik, Proceedings of Materials for Advanced Power Engineering, Liege, Belgium, 3−6 October 1994, Part I, pp. 685−704

[3] A. H. Rossette, Z. Mazur C, A. Demeulenaere, J.A. R. L. Hernández, *Applied Thermal Engineering* 29 (2009) 3056–3065

[4] H. Harada, Y. GU, *4th World Materials Research Institute Forum (WMRIF)*, Institute of Metal Research (IMR), Shenyang, May 24, 2011

[5] D. S. Rickerby, H. C. Low, *4th European Propulsion Forum*, 16 1-8 June, 1993, Royal Aeron. Soc. Bath, 1993

[6] C. G. Levi, *Current Opinion in Solid State and Materials Science* 8 (2004) 77−91

[7] A. K. Saini, D. Das, M. K. Pathak, *Procedia Engineering* 38 (2012) 3173–3179

[8] G. A. El-Awadi, S. Abdel-Samad, A. F. Waheed, *Arab Journal of Nuclear Science and Applications* 45(4) (2012) 298−308

[9] P. Bengtsson, C. Persson, *Surface and Coatings Technology* 92 (1997) 78–86

[10] G. W. Schaefer, R. Gadow, Proceedings of the 23rd Annual International Conference on Advanced Ceramics and Composites, Cocoa Beach of Florida, Jan. 1999

[11] C. J. Friedrich, R. Gadow, M. H. Lischka, Proceedings of the 25th Annual International Conference on Composites, Advanced Ceramics, Materials, and Structures: B, Cocoa Beach of Florida, Jan. 2001

[12] D. Stöver, C. Funke, *Journal of Materials Processing Technology* 92-93 (1999) 195–202

[13] Kh. G. Schmitt-Thomas, H. Haindl, D. Fu, *Surface and Coatings Technology* 94-95 (1997) 149–154

Journal of New Technology and Materials
JNTM
Vol. 05, N°02 (2015)20-23

OEB Univ. Publish. Co.

Getting ferromagnetic metallic nanofilms for information recording on the magnetic moments of the electrons

V. P. Panaetov

High-mountain Geophisical Institute, Kabardino-Balkarian Republic. Nalchik, street Lenin 2. 360004. Russia

e_mail: Vladimir.panaetov@gmail.com

Received date: July 03, 2015; revised date: October 31, 2015; accepted date: November 13, 2015

Abstracts:

The ferromagnetic nanofilms are promising for recording information by means of electron spins. The preparation of such films is technologically very cheap. It is assumed in such matrices can be a huge recording density information. But the main difficulty was the fact that the magnetic structure of the films depends on technological parameters of the film. The magnetic structure of films, prepared at different deposition, differ from each other. We have theoretically calculated parameters of the films in which there is a given domain structure. This theory has been tested experimentally. The films were produced, in which the observed magnetic image in advance was calculated by us. The possibility of obtaining a magnetic structure has allowed us to explore the rotation of the magnetization vectors in the domains

Keywords: Domain, walls, magnetization, electron, spin, energy, anisotropy.

1. Introduction

With the emergence of new trends in the field of microelectronics "spintronics" [1] dramatically increased the importance of studying the magnetization reversal of ferromagnetic nanofilms. Until now, the process of magnetization reversal is not fully understood. The ferromagnetic films may be suitable for the information recording via the magnetic moments of the electrons. Changing the domain structure and the distribution of the magnetic moments of the entire surface of the film takes place during the magnetization reversal of ferromagnetic metallic nanofilms. The distribution of the magnetic moments of the electrons can be seen in the distribution of the magnetization vectors on the surface of the film. The micro-magnetization process can be observed only at high magnification with a transmission electron microscope.

Part of the research program of search the minimum and maximum values of energy in thin films, they were held in Irkutsk State Pedagogical Institute in the laboratory of magnetic phenomena. Experimental results have been obtained with an electron microscope UEMV-100K (universal electronic microscope, an accelerating voltage of 100 kV, the increase is not less than 10^5-fold) and additional devices for monitoring the magnetic structure in the electron microscope. All devices are made by the author. Analyses of the results were performed in the laboratory of nanophysics and electronics in the Kabardino-Balkaria University and the Laboratory of microphysics of particles in High Mountain Geophysical Institute, in Kabardino-Balkaria, Nalchik, Russia.

So, to study the rotation of the magnetization vectors in the films we needed to have on screen been has at least three domains. Conveniently for this purpose can be the films with double-walls found in [2] Domains must be very narrow. The distance between the domain walls should be about 0.5 – 1.0 micron. We have obtained a film with such a magnetic structure. Thus, the necessary conditions have been met: a sufficient increase in the microscope and of the required magnetic structure. This article describes a method of producing films with a given magnetic structure. Technological parameters of the films were calculated.

2. Calculation of energy interacting homogeneous walls in films

To obtain a film with a given magnetic structure we have chosen theoretical model of such a structure. In our view, the most of appropriate and simple model of double walls Bloch and Neel there is the model of Kaczer [3]. Evaluation energy of the walls is made depending on the distance between them in the films of nickel, cobalt and alloy $Ni_{0,90}$-$Fe_{0,10}$. In the calculation were used the parameters of films: film thickness t, the saturation magnetization I, constant of perpendicular anisotropy $K_\perp$, who have real films with dual of domain walls. To calculate the energy were used by the expression to a double-walls Bloch and Neel (E_B, E_N) [3].

$$E_B = 2\gamma_B t \pm 4\gamma_B t \cdot e^{-s/\delta} \mp \frac{2\pi^2 I_s^2 t^2 \delta^2}{s^2}, \quad (1)$$

$$E_N = 2\gamma_N t \pm 4\gamma_N t \cdot e^{-s/\delta} \mp \frac{4\pi^2 I_s^2 t^2 \delta^2}{s^2}, \quad (2)$$

Where γ_B and γ_N - the energy density without the interaction of individual walls Bloch and Neel; t - film thickness; s - distance between the walls; δ - the width of one wall; I_s - the saturation magnetization. The upper signs in equations (1) and (2) correspond to the same rotation of the magnetization vectors in the two walls; bottom - opposite the direction of rotation of the magnetization vectors in the two walls.

Kaczer [3] has made calculations for massive materials. With reference for the films we used density of superficial energy of walls from [4]. In thin ferromagnetic films this energy develops not only of exchange energy and energy uniaxial anisotropy. Existing in films of the internal tensions and other factors (for example, of inclined deposition) result in occurrence perpendicular of anisotropy, characterized constant K⊥. Surface energy of the perpendicular anisotropy for walls Bloch in film is equal: γ =0, 3•K⊥ [5]. In view of it, the density of superficial energy for walls Bloch and Neel will be written down, accordingly:

$$\gamma_B = A(\frac{\pi}{\delta})^2 \cdot \delta + \frac{K_{II}\delta}{2} + \frac{\pi I_s^{\,2} \cdot \delta^2}{t+\delta} + 0{,}3\,K_\perp \cdot \delta \quad , \quad (3)$$

$$\gamma_N = A(\frac{\pi}{\delta})^2 \cdot \delta + \frac{K_{II}\delta}{2} + \frac{\pi I_s^{\,2} \cdot \delta t}{t+\delta} + K_\perp \cdot \delta , \quad (4)$$

Where A – is constant of the exchange energy; K_{II} - is constant uniaxial anisotropy in a plane. Energy of double walls was defined by minimization of expressions (1) and (2) concerning width of wall δ and distance between walls s. At account the following value of parameters were used: $A = 0{,}9 \cdot 10^{-11}$ J/m; t=10-70 nm; K⊥ = (2-10) 10^4 J/m^3; K_{II} = 2 10^2 J/m^3.

Type walls depend on the film thickness and the value of the perpendicular anisotropy. In this regard, various alloys were chosen in order to be able to obtain samples with different values of the constants perpendicular anisotropy. For example, films with negative magnetostriction can be using mechanical stresses set certain constant value perpendicular anisotropy. Furthermore, the magnitude of the linear density of the magnetostatic energy of domain walls (in the expressions 1 and 2) $(2\pi^2 \cdot I_s^2 \cdot t^2 \cdot \delta^2) / s^2$ depend on the value of the saturation magnetization. Thus, for the study were selected alloys with different values of the saturation magnetization and magnetostriction, Ni (I_s=0,48 A/m); $Ni_{0,90}$-$Fe_{0,10}$ (I_s=0,65 A/m); Co (I_s=1,40 A/m).

The following results were obtained from theoretical calculations of the energy for the Bloch walls in films.

The energy for double walls Bloch with an opposite direction of rotation is greater than the total energy of non-interacting isolated walls, the linear density is equal 2γt (Figure. 1a, b). The value energy of for Bloch double walls with the same direction of rotation of the magnetization vectors in the walls is less than the sum of energies of the isolated walls (Figure. 1c, d). Results are shown for films of a thickness of nickel 10 and 70 nm.

From results of account follows, that the double walls such as walls Bloch with an identical direction of rotation of vectors magnetization of saturation in them are energetically more favorable, than walls with unequal direction of rotation I_s. It is visible, that at distance s=10^3 nm linear density of energy of interaction of walls for nickel films aspires to zero.

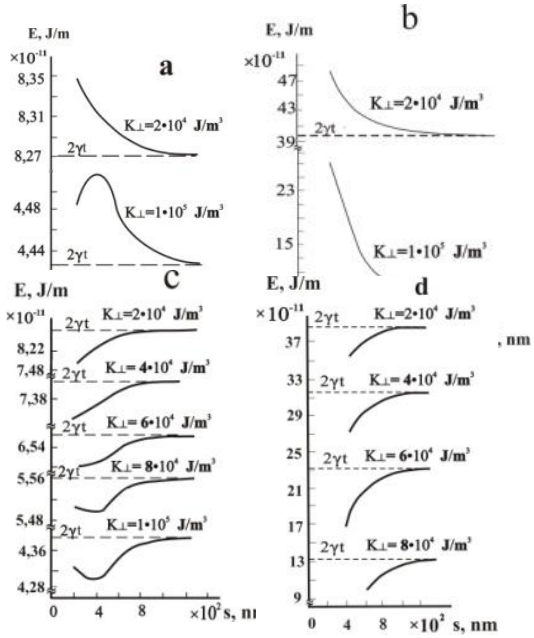

Figure 1. The linear energy density of two adjacent walls of the Bloch for films Ni depending on the distance between them and the values of the thickness of the film: a, b - t = 10 nm; c, d - t = 70 nm; a, b - the Unequal direction of rotation of the magnetization; c, d - the same direction of rotation. The dotted line in the chart shows the energy density of the two insulated walls with identical magnetization rotation.

Energy of walls is equal to the sum energy of the isolated walls, that is at distances s=10^3 nm the walls can be considered as isolated. The figure. 1c corresponds films nickel by thickness 70 nm and K⊥ > 8•10^4 J/m^3. On the diagram dependence of linear density of energy of walls with an identical direction of rotation of vectors magnetization of saturation in them from the distance between the next walls there is a minimum of value energy. It specifies an opportunity of existence in films with equilibrium magnetic structure of double walls, distance between which should be about 400 nm. For films of an alloy $Ni_{0,90}$-$Fe_{0,10}$ in an interval of thickness from 10 nm up to 80 nm was not found of minimum of energy for stable double walls Bloch in absence of an external magnetic field.

On depending linear energy density of domain walls of Neel from distance between them (figure 2) there is a minimum value of energy. In double of walls with identical direction of rotation of the magnetization I_s in them, has occurs minimum, when distance between them s ~ 200 nm (figure 2a), for walls with varying rotation of the magnetization - about ~ 400 nm (figure 2b).

That is, in the films Ni, Co, Fe Ni of thickness 10 nm with a small value constant perpendicular anisotropy, may exist equilibrium magnetic structures type Neel with distance between them ~ 200-400 nm.

The formation at the curve of the minimum energy linear density the from distance between walls and for the Bloch walls and for the Neel walls due to the fact that the energy density of the linear expression (1, 2) includes components of this energy (the second and third terms) with opposite signs, having unequal dependence on the distance between the walls.

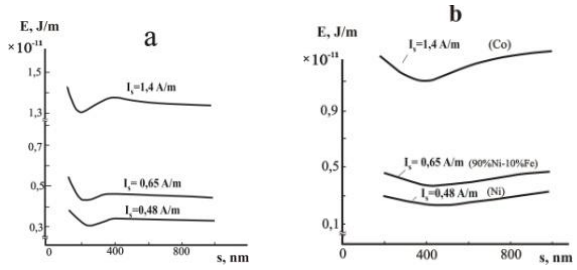

Figure 2. Dependence of energy of walls Neel from distances between them: a - identical rotation **I.**; b - unequal rotation **I.**. At account was the value $K_\perp = 2\cdot10^4 J/m^3$, $K_{II}=2\cdot10^2 J/m^3$

Thus, for films of cobalt 10 nm in thickness in table 1 shows the values of the energies $4\gamma_N t\, e^{-\delta}$ and $2\pi^2 I_s^2 t^2 \delta^2/s^2$ depending on the distance between them for the same rotation in the walls I_s Neel. It is seen that these energies are approximately equal to each other (in absolute value) at distances s ~ 200 nm. In this interval, and was found the minimum energy (figure 3).

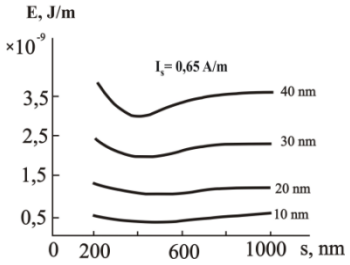

Figure 3. Dependence of energy of double walls Neel walls from distance between them for different thickness films. Structure films: $Ni_{0,90}$ – $Fe_{0,10}$, I_s = 0,65 A/m; $K_{II}= 2\cdot10^2 \cdot J/m^3$; $K_\perp = 2\cdot10^4 J/m^3$.

The distance between the walls of s, nm	$4\gamma_N t\, e^{-\delta}$ G /m	$\frac{2\pi^2 I_s t^2 \delta^2}{s^2}$ G /m
100	$+11{,}7\cdot10^{-14}$	$-11{,}7\cdot10^{-16}$
200	$+5{,}2\cdot10^{-17}$	$-8{,}7\cdot10^{-17}$
400	$+12{,}0\cdot10^{-29}$	$-3{,}8\cdot10^{-17}$
600	$+23{,}6\cdot10^{-38}$	$-2{,}7\cdot10^{-17}$
800	$+5{,}36\cdot10^{-46}$	$-3{,}8\cdot10^{-17}$
1000	$+1{,}0\cdot10^{-54}$	$-3{,}8\cdot10^{-17}$

Table 1.Dependent functions $4\gamma_N t\, e^{-\delta}$ and $2\pi^2 I_s^2 t^2 \delta^2/s^2$ the distance between the walls of s ,

Linear dependence of the energy density of interacting Neel walls of the distance between them for different film thicknesses (composition $Ni_{0,90}$-$Fe_{0,10}$, I_s = 0,65 A / m) is shown in figure 3. It is seen that with increasing film thickness energy Neel walls in the case of unequal direction of rotation of the magnetization vectors in adjacent walls increases. The same conclusion was reached for the wall with the same rotation I_s.

Anisotropy energy and the magnetostatic energy may vary with the distance between the domain walls, which follows from the expressions for the linear energy density of domain walls (2). The numerical accounts given in the table 1, show, that magnetostatic energy at the certain distances brings in the contribution much greater, than energy anisotropy. For example, for walls Bloch with identical rotation I_s the reduction magnetostatic of energy is caused by partial short circuit of a stream of magnetization when approaching walls. Walls called homogeneous that do not have cross-tie walls.

The picture (in figure 4) ripples magnetization (the dispersion of the magnetic anisotropy) abruptly appears and can say with confidence that this is the Neel's wall. It shows there is the interacting not only between the double walls, but also between the pairs of domain walls. Experimental measurements of the distance between the double walls are consistent with our calculations. Between pairs of double domain walls having domains with magnetization vectors in them, directed at an angle of 45^0 to the axis of easy magnetization. In our opinion, this phenomenon is associated with a decrease in magnetostatic energy.

At a film thickness of 20 nm and a low value $K_\perp$ the magnetization vector is not profitable to leave the plane of the sample, due to the demagnetization factor. This is analogous to the way in films of thickness of about 45-65 nm, decreasing the magnetostatic energy of the sample as a whole is due to the emergence of cross-links.

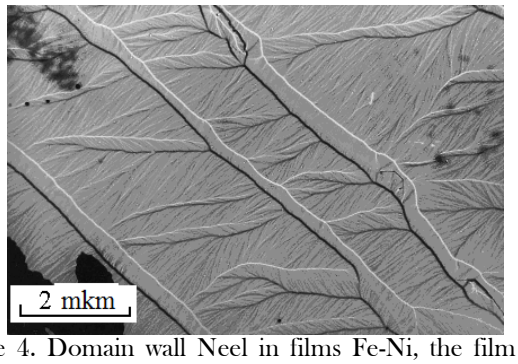

Figure 4. Domain wall Neel in films Fe-Ni, the film thickness t = 20 nm

Figure 5 shows the magnetic structure of the nickel film obtained on a cold substrate (300 K). In the image you can see that there is no magnetization ripple. The image of magnetic structure is not clear, there are many defects. But in this case we have a large constant perpendicular anisotropy ($K_\perp = 8\cdot10^4 J/m^3$). Comparison of experimental and calculated data for films of nickel thickness of 70 nm and $K_\perp = (8\text{-}10)\cdot10^4$

J / m^3 gives grounds to assume that in these films take place Bloch wall (walls a large component of the distribution of the magnetization vectors of the film thickness) with the same direction of rotation I. The dispersion of the magnetic anisotropy of the film surface is missing (ripple magnetization is not observed).

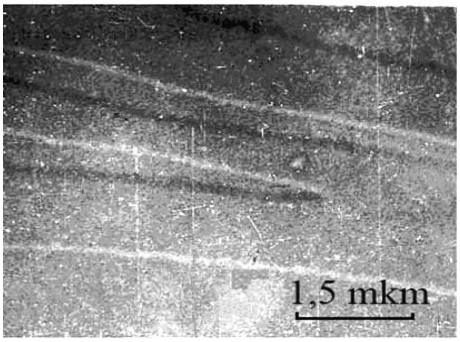

Figure5. Domain walls in films of nickel, previously were demagnetized in variable magnetic field with decreasing field to zero: film thickness t=70 nm; constant of perpendicular anisotropy $K\perp = 8 \cdot 10^4$ J/m^3.

3. Results

1. Developed and tested technique for obtaining ferromagnetic films with a given magnetic structure. A similar procedure for the preparation of films is offered for the first time in the world literature. On the curve of the linear energy density, depending on the distance between of domain walls was detected a minimum of energy. Minimum energy means that at the given parameters of the film there are stable double walls. Films with double walls were received and investigated by us in [6]. The results were obtained from this work, by determination the rotation of the magnetization vectors in the domain walls.
From the analysis of the above calculation results, the following conclusions:

2. In films (thickness ~70nm), with constant $K\perp$ (~ $8 \cdot 10^4$ J / m^3) are energetically more favorable double walls Bloch with the same direction of rotation of the magnetization **L**.

3. In nickel films (thickness ~10nm) may occur Neel double walls as with the same direction the rotation of the magnetization **L** (distance s ~ 200nm) and unequal direction of rotation of the magnetization (s ~ 400nm)

4. The experimental results have confirmed our theoretical calculations. Figures 4-5 show the experimental double walls.

5. This method can be recommended for the production of films with the required parameters, both for scientific purposes and for industrial production.

6. Thus, summing up the above results can to make the main conclusion of this work:
on the basis of theoretical and experimental research, we developed a methodology for producing ferromagnetic films with a given magnetic structure.

References

[1] A.V. Ognev, A.S. Samardak "Spintronics: physical principles, devices, future". Bulletin FEB RAS. № 4. 70-80. (2006).
[2]. H.J. Williams, R.C. Sherwood "Magnetic Domain Patterns on Thin Films" *J. Appl. Phys.* V. 28 548-555 (1957).
[3]. I Kaczer, "Theory of Double Bloch Walls in Thin Films". *J. Appl. Phys.* 29 3 569-572 (1958).
[4]. S. Middelhoek, "Ferromagnetik Domain in Thin Nickel iron Films". *Ph D Thesis* University of Amsterdam 78 (1961).
[5]. E.A. Gorohov, V.P. Karabanova, V.I. Popov, "The impact on the structure of the perpendicular anisotropy of domain walls in thin ferromagnetic films" *Fiz.* 30 6 1287-1290 (1970).
[6]. V.P. Panaetov, "Experimental investigation of the magnetic structure of domain walls in thin ferromagnetic films *"Physics of the Solid State*" 51 10 2064-2068 (2009).

Journal of New Technology and Materials
JNTM
Vol. 05, N°02 (2015)24-27

OEB Univ. Publish. Co.

The barrier height and the series resistance of Ag/SnO_2/Si/Au Schottky diode determined by Cheung and Lien methods

Mostefa Benhaliliba

Material Technology Department, Physics Faculty, USTOMB University, BP1505 Oran, Algeria.

mbenhaliliba@gmail.com

Received date: August 24, 2015; revised date: December 05, 2015; accepted date: December 06, 2015

Abstract

Electronic parameters of Ag/SnO_2 /Si/Au Schottky diode (SD) determined by Cheung and Lien methods are extracted using the current-voltage (I-V) and the capacitance-voltage (C-V) characteristics. Such SD is fabricated by the spray pyrolysis and the metallic contact is achieved by thermal evaporation process in vacuum. To determine more parameters of SD, the quantities like dV/dlnI, H(I) and Ga(V) are introduced. The non-ideal behavior of SD is confirmed, n=4.86 (n>1), the barrier height ΦB and the series resistance Rs are found to be 0.62 V and 585 Ω (by dV/dlnI), 524.5Ω (by H(I). The use of C-V and C^{-2}-V plots allow us to determine the density of acceptor (Na) and diffusion potential (Vd), at a kept frequency of 1MHz, of 7.8 1021 cm-3 and 0.49 V respectively. The profile of C-V, measured at various frequencies, reveals a p type of as fabricated SD where tin oxide layer is doped with 4% indium.

Keywords: Tin oxide; Indium doping; Spray pyrolysis, Schootky diode; Ideality factor; I-V measurement; C-V characteristics.

1. Introduction

Films and devices based on a wide band gap tin oxide semiconductor are largely studied due to its several properties. Such diodes have attracted many researchers and find applications in optoelectronics and sensor devices [1-2]. Lately, researchers have requested that SnO_2 could exhibit many qualities in opto-electrical applications. Further, these properties are improved when it is doped with metallic cations like aluminium, indium, antimony, zinc and iron [3-8]. Hydrothermal method, sputtering and the pray pyrolysis process are among the main used deposition techniques [9-11]. In order to discover the electronic properties of Schottky diode based on tin oxide doped with indium, the Ag/SnO_2 /Si/Au SD is fabricated and the I-V and C-V are measured under dark and room temperature conditions.

2. Fabrication details of Ag/SnO_2/Si/Au Schottky diode

The layers of tin oxide have been grown on n type silicon by ultrasonic spray pyrolysis technique USP at 300 °C. The doping source was indium (3+) chloride (InCl3), the ratio In/Sn was fixed at 4% in the solution. Both precursor and doping compound were dissolved in methanol at room temperature as previously cited [4, 12]. The gold contact, of thickness of 120 nm, was deposited on the film by thermal evaporation at pressure of 1.5 x 10−5 Torr. The I-V and C-V characteristics are achieved by employing Keithley and Agilent impedance analyzer set up respectively as reported previously [4, 12].

3. Results and discussion

In our study, the methods developed by Cheung et al. and Lien et al. have been applied to extract electronic parameters [14-15]. For a Schottky diode with a uniform oxide layer, it is reported that the relation between the applied forward bias and current

of the device is due to thermionic emission current and it is given by,

$$I = I_0\left[\exp\left(\frac{qV}{nkT}\right)-1\right] \quad (1)$$

As known, the ideality factor is n and the saturation current is I_0 . The figure 1 depicts the I-V (semilog) characteristics of Ag/SnO_2/Si/Au SD in dark and room temperature. The measurement of current is achieved in the {-2V, +2 V} bias range. As shown by the profile, the SD exhibits a slight rectifying behaviour, where the rectifying factor is defined as R= I(2V)/I(-2V), (R >200) while the as-fabricated SD based on SnO_2 doped with 6% In has presented a high rectifying factor (R>420) and ideality factor (n~2.7) was less than that obtained here (4.86), as mentioned in previous work [12]. The forward current increases exponentially with voltage as expressed by eqn.1, but the reverse bias current shows a poor saturation for low reverse applied

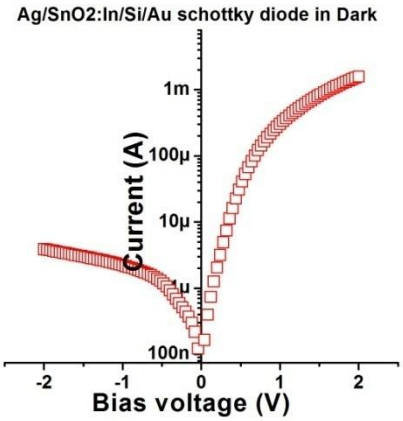

Figure 1. Under dark, the current-voltage characteristics plotting of Ag/SnO_2/Si/Au Schottky diode.

voltages and increases slowly.

$$n = \frac{q}{kT}\frac{dV}{d\ln(I)} \quad (2)$$

I_0 is easily extracted from the extrapolation of the linear portion of semi-log I-V and is given by,

$$I_0 = AA^*T^2\exp(-\frac{q\phi_{B0}}{kT}) \quad (3)$$

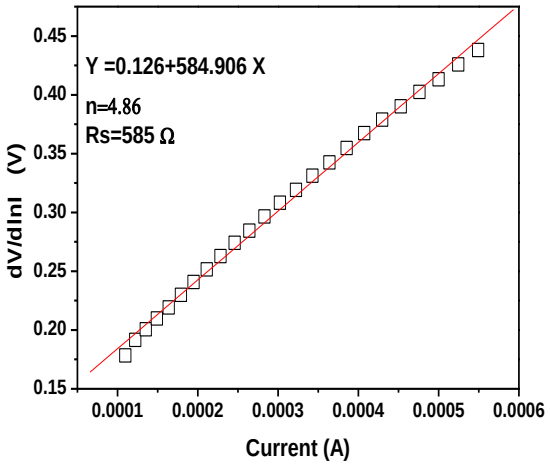

Figure 2. Sketch of dV/dlnI vs. current of Ag/SnO_2 /Si/Au Schottky diode fabricated by spray pyrolysis process (the red solid line indicates the linear fit).

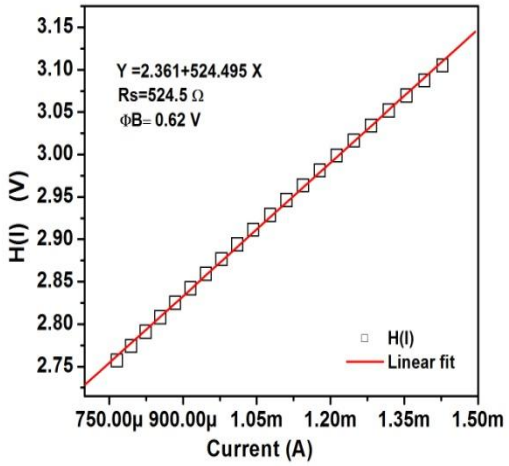

Figure 3. Plot of H vs. current of Ag/SnO_2/Si/Au Schottky diode fabricated by spray pyrolysis process (linear fit is displayed by a red solid line).

For the voltage greater than V> 3kT/q, the ideality factor and the saturation current, which are extracted from the linear fitting of LogI-V curve, are found to be 3.34 and 0.4 µA. Based on these results, our fabricated SD exhibits a non-ideal behavior due to n>1 due to presence of series resistance and interface states which are present between the SnO_2 layer and the silicon substrate. As shown in figures 2 and 3, the linear fit of the forward I-V permit us to know accurately the value of ideality factor, series resistance and barrier height for the large measured currents. It is explained by the non-ideal behavior of the SD which is caused by the

interface existence in the metal-semiconductor junction. In this behavior of our SD, n increases a little (n=4.86), Rs= 585 Ω by (dV/dlnI method) and 524.5 Ω by (H(I) method) and a barrier height of 0.62 V.

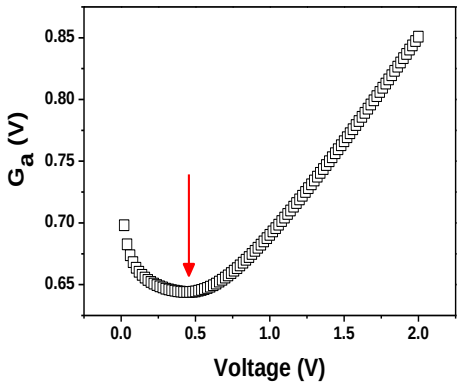

Figure 4. The plotting of the quantity G_a vs. bias voltage of Ag/SnO_2/Si/Au Schottky diode in dark condition and room temperature (the minimum Ga(V_0) is indicated by red arrow).

Whereas, the respective obtained values of Rs and Φ_B are found to be 508 Ω and 0.58 V for the case of 6% In as reported earlier [12]. The Cheung-Cheung method is employed to determine some parameters in the non-ideal behavior of the diode [15];

$$\frac{dV}{d\ln I} = R_s I + n(\frac{kT}{q}) \quad (4)$$

The H(I) function versus current is expressed as follows [13],

$$H(I) = V - (\frac{nkT}{q})\ln(\frac{I}{AA^*T^2}) \quad (5)$$

The plotting of Ga vs. bias voltage is sketched in figure 4. Furthermore the function H is given by,

$$H(I) = n\Phi_B + R_s I \quad (6)$$

The figure 5 shows the capacitance-voltage of as fabricated SD within the -5V, +5V voltage range for several frequencies100kHz- 1MHz.

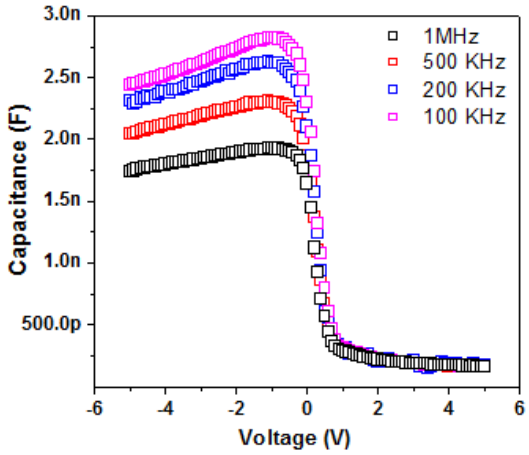

Figure 5. The capacitance-voltage profile of Ag/SnO_2/Si/Au Schottky diode at various frequencies 100kHz-1MHz.

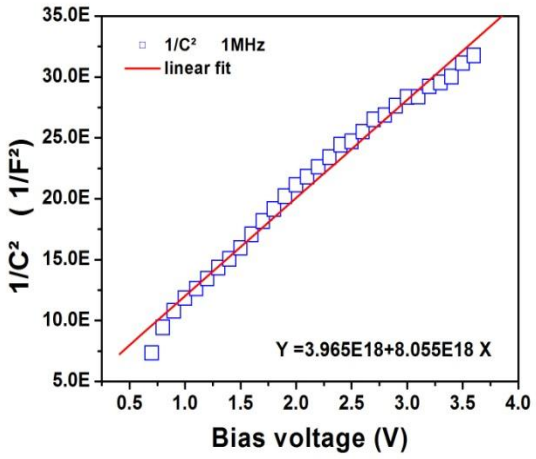

Figure 6. The variation plot of C^{-2}-V of Ag/SnO_2/Si/Au Schottky diode in dark and room temperature condition. Red solid line indicates the linear fit and its equation is written in the bottom ($E=10^{18}$ in y-axis).

The Lien method is based on the plotting of G function defined [14] by;

$$G_a = \frac{V}{a} - \frac{1}{\beta}\ln(\frac{I}{AA^*T^2}) \quad (7)$$

Where the barrier height and series resistance are defined as follows;

$$\phi_B = G(V_0) + \frac{V_0}{a} - \frac{kT}{q} \quad (8)$$

$$R_s = \frac{kT(a-n)}{qI_{min}} \quad (9)$$

Where the constant β=q/kT and a is integer parameter greater that n. Here, n is found to be 4.86, as indicated above and in the inset of figure 2, a is taken equal to 5 and the area value (A) of contact is found to be 0.018 cm^2. The constant (AA^*T^2) is of 80640 and the Richardson constant of n type silicon is 112 A /$Kxcm^2$. Thus, the following magnitudes V0=0.44 V, its corresponding current (Imin) is of 3.77 μA and G (V0) =0.64 V are determined from the figure 4. From eqn.8, the barrier height is then found to be 0.70 V and Rs, from eqn.9, is evaluated at 960.87 Ω[14].

$$\frac{1}{C^2} = \frac{2(V_d + V)}{q\varepsilon A^2 N_a} \quad (10)$$

The two values of Rs found by dV/dlnI and H(I) are close and different from that found by Lien method. This discrepancy might due to following reason that Cheung's methods are only applied for the non-linear part of the forward bias I-V characteristics and Norde functions (F-V) are applied for the full forward region of I-V curve of the diode. From the linear fit of C^{-2}-V throughout the equation displayed inside of figure 6, the concentration is easily determined using the eqn.10 [13]. It is found that N_a=7.8 10^{21} cm^{-3} and V_d =0.49 V.

Conclusion

The series resistance and barrier height of Ag/SnO_2/Si/Au Schottky diode in dark and room temperature condition have been measured and extracted using Cheung and Lien approximation methods. The non-ideal behaviour of Ag/SnO_2/Si/Au Schottky diode is confirmed n>1. Such situation of the non-ideal behavior, leads to think to the presence of the series resistance and the interface states. Cheung and Lien approximation techniques permit to confirm this statement by calculating the parameters cited above and found to be 524.5 Ω and 0.62 V. A p type of as fabricated SD where tin oxide layer is doped with 4% idium. The density of acceptor is found to be 7.8 10^{21} cm^{-3} and the diffusion potential is of 0.49V. A p type of as fabricated SD, with 4% In doping level, is revealed.

Acknowledgments

This work is supported by the Algerian Ministry of High Education and Scientific Research through the CNEPRU project No. B0L002UN310220130011, www.mesrs.dz, and www.univ-usto.dz. I would thank the Turkish lab. for their help.

References

[1]Sangyub Ie, Ji-Hwan Kima, Byeong Taek Bae, Dong-Hee Park, Ji-Won Choi, Won-Kook Choi, Thin Solid Films 517 (2009) 4015-4018.
[2]Wen Zeng, Tianmo Liu , Zhongchang Wang, Physica E 43 (2010) 633-638.
[3] J.S. Bhat, K.I. Maddani, A.M. Karguppikar, S. Ganesh, Nuclear Instruments and Methods in Physics Research B 258 (2007) 369-374.
[4]C.E. Benouis, M. Benhaliliba, F. Yakuphanoglu, A. Tiburcio Silver, M.S. Aida, A. Sanchez Juarez, Synthetic Metals 161 (2011) 1509-1516.
[5]Zhenguo Ji, Zhenjie He, Yongliang Song, Kun Liu, ZhiZhen Ye, Journal of Crystal Growth 259 (2003) 282-285.
[6]Yuan-Qing Li, Jian-Lei Wang, Shao-Yun Fu, Shi-Gang Mei, Jian-Min Zhang , Kang Yong, Materials Research Bulletin 45 (2010) 677-681.
[7] R.K. Mishra, P.P. Sahay, Ceram. Inter. 38 (2012) 2295-2304.
[8]M.A. Batal, F. Haj Jneed, Energy Procedia 6 (2011) 1-10.
[9]Liu D, et al. Gas sensing mechanism and properties of Ce-doped SnO_2 sensors for volatile organic compounds. Materials Science in Semiconductor Processing (2012), doi:10.1016/j.mssp.2012.02.015.
[10]F. de Moure-Flores, J.G. Quiñones-Galván, A. Hernández-Hernández, A. Guillén-Cervantes, M.A. Santana-Aranda, M. de la L. Olvera, M. Meléndez-Lira, Appl. Surf. Sci. 258 (2012) 2459-2463.
[11]C. Luangchaisri, S. Dumrongrattana, P. Rakkwamsuk, Procedia Engineering 32 (2012) 663-669.
[12]Mostefa Benhaliliba, Journal of Nano- and Electronic Physics Vol. 7 No 2, 02029(4pp) (2015).
[13]M. Benhaliliba, Y.S. Ocak, H. Mokhtari, T. Kiliçoglu, Journal of Nano- and Electronic Physics, Vol. 7 No 2, 02001(4pp) (2015).
[14]C.D. Lien, F.C.T. So, M.A. Nicolet, IEEE Trans. Electron.
Devices ED-31 (1984) 1502.
[15]S.K. Cheung, N.W. Cheung, Extraction of Schottky diode parameters from forward current-voltage characteristics, Applied Physics Letters, 49 (1986) 85-87.

Journal of New Technology and Materials
JNTM
Vol. 05, N°02 (2015)28-32

OEB Univ. Publish. Co.

Spectroscopic study of poly (vinylidene fluoride)/ poly (methyl methacrylate) (PVDF/PMMA) blend

F. Z. Benabid [A,*], F. Zouai [B] and A. Douibi [A]

[a] *LMPMP, Faculté de Technologie, Université Ferhat Abbas Sétif-1, Algérie*
[b] *Unité de Recherche Matériaux Emergents, Université Ferhat Abbas Sétif-1, Algérie*
[*] *Corresponding author, e-mail address: fzbenabid@yahoo.fr*

Received date: November 03, 2015; revised date: December 16, 2015; accepted date: December 17, 2015

Abstract

Poly (Poly (vinylidene fluoride)/poly (methyl methacrylate) blends casted in DMF could be used in the conservation of historic structures (monuments) exposed to atmospheric agents or as a coating to replace and maintain parts or missing pieces. This study deals with the effect of blending PVDF to PMMA to enhance their properties using FTIR and UV-visible spectroscopy. In FTIR spectra, it was found that PVDF/PMMA blend casted in the Dimethylformamide (DMF) showed the superposition of the spectra of all compositions, with the exclusion of any chemical reaction between two polymers or the presence of the double bonds characteristic of PVDF dehydrofluoration. The UV-visible spectroscopy before and after exposure to artificial weathering, showed that the PVDF is very stable (the invariant absorbance values at 200nm wavelength after the equivalent of two years of aging). In contrast, the absorbance of PMMA has changed at the same wavelength explaining its tendency of degradation.

Key words: Blend, PVDF, PMMA, Monuments.

Introduction

The The conservation and protection of historic monuments or culturally significant structures have recently attracted much attention from material scientists [1]. A few years ago, various synthetic polymers have been widely used in the treatment of construction materials of historical monuments for consolidation and conservation of such structures [2]. Using polymeric coatings for this area has created serious challenges for the surface science and technology. Some of the challenges are as follows [3, 4]. Van Hees and Brocken [5] evaluated the salt growth in brick masonry specimens, coated with a water repellent, during a salt crystallization test. They demonstrated that the behavior of different salts on development of salt damages is completely different. However, it is demonstrated that the adsorption of dusts suspensions and water-soluble air pollutants decreases with increasing hydrophobicity of the surface of building materials [1]. The fluorine substitution of the hydrogen atoms present in a macromolecular chain improves the heat resistance and chemical resistance, delays or inhibits flame propagation, lowering the critical surface tension and exalts the dielectric characteristics [6]. Acrylic resins undergo deterioration face conditions under UV radiation and their climatic exposure causes degradation of their structure. However, their physical characteristics and low price always consider important research topics. Estevão Freire et al. [7] have studied the morphological, thermal and non-isothermal crystallization behavior of the PVDF and its blends with the PMMA processed in low (LSM) and high (HSM) shear mixers using the differential scanning calorimetry (DSC). The addition of PMMA into PVDF increases of relative ß phase content independent of the processing conditions. The validity of the modified Avrami and Kolmogorov–Johnson–Mehl–Avrami (KJMA) models for the non-isothermal crystallization of PVDF/PMMA blends were discussed. The results showed a shift in the PVDF crystallization/fusion peak to lower temperatures. The activation energies for crystallization of PVDF and its blends evaluated through the isoconversional method using Friedman's approximation were higher for samples processed in the LSM. Jing Sun et al. [8] have studied the modification on crystallization of PVDF by solvent extraction of PMMA in PVDF/PMMA blends. The mass crystallinity (χ_c) and further, the β-phase content ($F_{(\beta)}$) of PVDF, were studied for the blend films with different mass ratios.

DSC, FTIR and XRD measurements all indicated that χ_c, $F_{(\beta)}$ and even the content of α-phase ($F_{(\beta)}$) decreased with the addition of PMMA and with the extraction of PMMA, both χ_c and $F_{(\beta)}$ increased while $F_{(\beta)}$ decreased. In this research work, the focus was on the development of films of PVDF and PMMA blends and their spectroscopic analysis (FTIR and UV-visible spectroscopy).

Materials and methods

PVDF (Hylar 5000), special coating as a white powder, manufactured by Ausimont, Italy [9] and PMMA (Vedril ® Spa-Resina Metacrilica) manufactured by Mont Edison, Italy were used [10].

The PVDF/PMMA films were obtained by casting each polymer separately in with 1 % concentration of the polymer in the solvent (DMF) at temperature, 70°C (see table1).

Table 1: Different compositions in volume percentage proposed in this study

PVDF (%)	100	90	80	70	60	50	40	30	20	10	0
PMMA (%)	0	10	20	30	40	50	60	70	80	90	100

Moisture, temperature and ultraviolet radiation contribute to material degradation. Accelerated weathering test (Xeno Test) is the simulation of these conditions using special environmental chambers and instruments in order to speed up the weathering process and measure its effects on parts, components, products, and materials. On the other hand, the Salt spray testing is a test method for evaluating a product or a coating resistance to corrosion in the face of extended exposure to a saline, or salted, spray.

FTIR spectroscopy

Fourier-transform infrared spectroscopy (FTIR) spectra were recorded by means of a Perkin Elmer Spectrum 1000 spectrometer with a wavenumber resolution of 4 cm^{-1} in the range from 450 to 4400 cm^{-1}, using attenuated total reflection. Each spectrum results from an average of 200 scans to detect any changes in the chemical structure of various compositions of PVDF/ PMMA blends before and after exposure to artificial weathering (Xeno Test and Salt Spray) according to ISO 11507:1997(F) and ISO 7253:1996(F) respectively.

UV-visible spectroscopy

The UV-visible spectroscopy was performed using a Unicam UV 300 spectrophotometer to determine the evolution of the absorbance of various compositions of PVDF/PMMA blends before and after exposure to artificial weathering (XENO Test and Salt Spray).

Results and discussion

FTIR spectroscopy

FTIR spectra of PVDF/PMMA blends showed the spectral superposition of all the compositions where the exclusion of any chemical reactions between the two polymers. The results of the FTIR of the PVDF/PMMA blend solutions in the DMF (Fig.1, 2 and 3) showed the appearance of a band at 3470 cm^{-1} for the PVDF and at 3538 cm^{-1} for the PMMA corresponding to the hydrogen bonds of the hydroxyl group initiated by the solvent. The DMF is also the source of the occurrence of the stretching vibration of C=O amide 1673 cm^{-1} and for the PVDF to 1675 cm^{-1} for the PMMA.

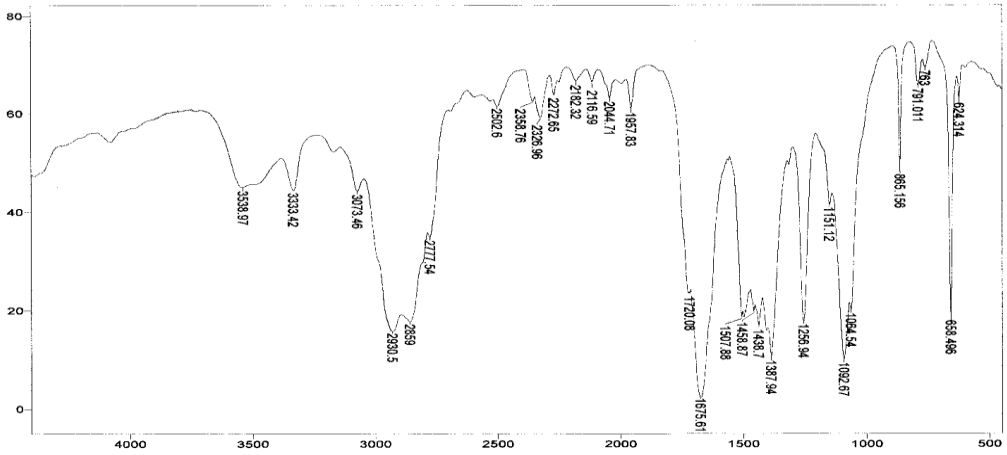

Fig. 1: Evolution of IR transmittance (%) of the PMMA casted in DMF as a function of the wave number (cm^{-1})

In the films of PVDF/PMMA blend before and after exposure to artificial weathering and to the salt spray it is noted that the bands at 510, 839, 880 and 1406 cm^{-1} are those of the β crystallinity phase of the PVDF [11, 12]. The α-phase is identified by the presence of peaks at 763 and 948 cm^{-1} [13, 14]. It should be noted that according to the literature [15, 16], the increase in the temperature reduces the presence of the crystallization of the β phase and it is clear that for a high proportion of this phase it must perform complete drying films at 75 ° C. The strong band at 1233 cm^{-1} is due to CF_2 and while the CH bonds showed peaks at 2980 and 3022 cm^{-1}. The deformation of CH_2 bonds is located at 1429 cm^{-1}.

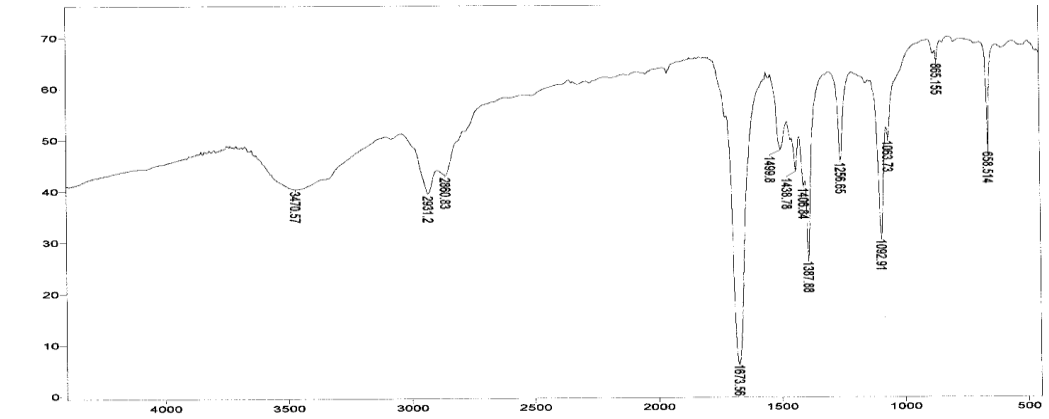

Fig. 2: Evolution of IR transmittance (%) of the PVDF casted in DMF as a function of the wave number (cm^{-1})

Concerning the PMMA, a strong peak at 750cm^{-1} present identifying the ρ ($C-H_2$) rocking; The C-O-C bond (ether ester) is indicated by the presence of peaks at 1151 and 1256 cm^{-1}.

The peaks at 1438 and 1458 cm^{-1} are characteristics of C-H bonds(bending) and the one at 1720 cm^{-1} is due to presence of carbonyl group (C=O).

Peaks characterizing the vibration of symmetric and asymmetric –CH stretching are at 2859 and 2930 cm^{-1} respectively.

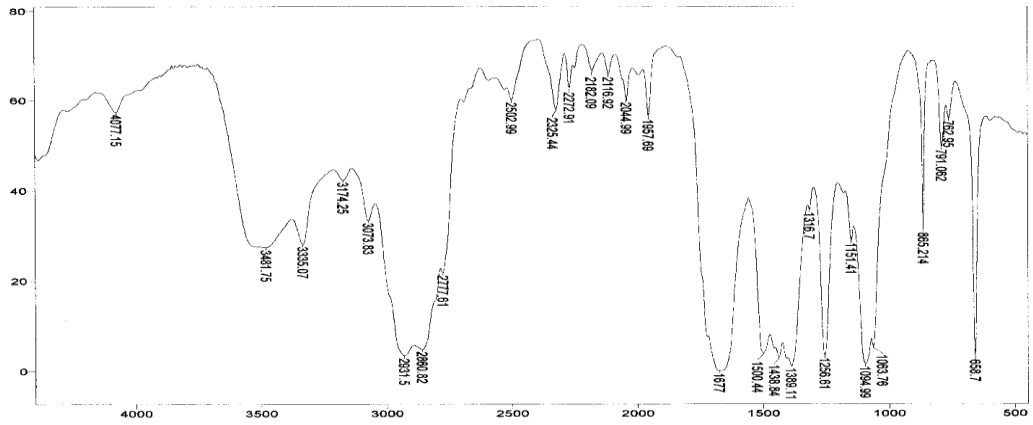

Fig. 3: Evolution of IR transmittance (%) of the different compositions of the PVDF/PMMA (50/50) casted in the DMF as a function of the wave number(cm^{-1})

UV-visible spectroscopy:

In table 2 and Fig.4 showing the absorbance variations as a function of the different compositions of the PVDF/ PMMA blends in solution in DMF before and after exposure to artificial weathering and salt spray.

Table 2: Absorbance variation versus different compositions of PVDF/PMMA blends at before and after exposure to artificial weathering at wavelength of 200 nm.

Absorbance	PVDF	PMMA
Before exposure	0,914	1,690
After exposure	0.927	0.565

Table 2 concerns films, before and after exposure to artificial weathering, it has been observed that for the PVDF, the absorbance value is the same compared to the reference film (before aging) (0,914) and that after exposure to artificial aging (0,927) which explains the stability of PVDF even after the equivalent of two years of aging.

However, for the PMMA, the absorbance values changed compared to the reference film (before aging) (1,690), that after exposure to artificial aging (0.565) which explains the tendency of PMMA degradation.

Table 3: Absorbance variation versus different compositions of PVDF/PMMA blends at before and after exposure to salt spray a wavelength of 200 nm

Absorbance	PVDF	PMMA
Before exposure	0,914	1,690
After exposure	0.905	0.661

Table 3 concerns films, before and after exposure to salt spray, it has been observed that for the PVDF, the absorbance value is the same compared to the reference film (before exposure) (0,914) and that after exposure to salt spray (0,905) which explains the stability of PVDF .

However for the PMMA, the absorbance values changed compared to the reference film (before exposure) (1,690), that after exposure (0.661) which explains the tendency of PMMA degradation.

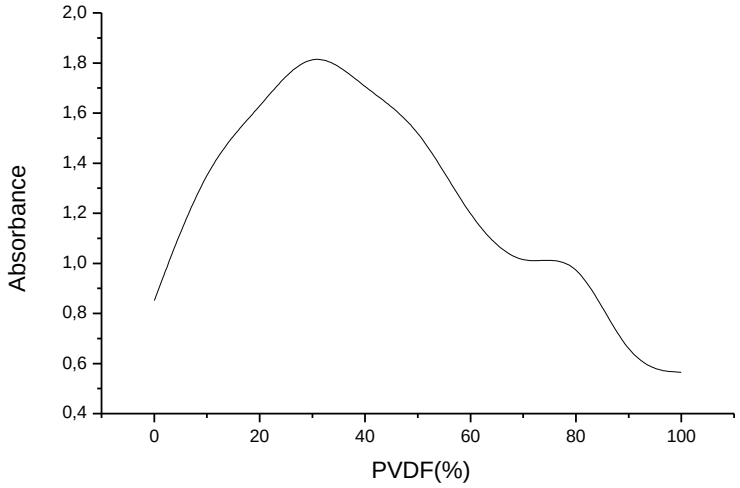

Fig.4: Absorbance Evolution as a function of the different compositions of PVDF/PMMA blend at a wavelength of 200 nm

The figure 4 which represents the absorbance variation as a function of the different compositions of the PVDF/PMMA blends dissolved in the DMF showed that there is a synergism with an optimum at 30/70.

Conclusion

From the different results obtained, it can be concluded that infrared spectroscopy (FTIR) of PVDF/PMMA blends casted in the DMF showed the superposition of the spectra of all compositions where the exclusion of any chemical reactions between two polymers or the presence of the double bonds characteristic of dehydrofluorination. On the other hand, the PVDF/PMMA studied blend showed the presence of two crystallinity phases α and ß. UV visible spectroscopy showed that the PVDF is very stable (the invariant absorbance values at 200 nm wavelength) after the equivalent of two years of aging. In contrast, the absorbance of PMMA has changed at the same wavelength (200 nm), which explains its tendency to degradation. The UV-visible spectroscopy showed that for the various compositions of the PVDF / PMMA blends dissolved in the DMF, the absorbance increased and therefore the solubility of the blend.

References

[1] M. Sadat-Shojai and A. Ershad-Langroudi, "Polymeric Coatings for Protection of Historic Monuments: Opportunities and Challenges", *Journal of Applied Polymer Science,* **112**, (2009) 2535-2551

[2] M. Favaro, R. Mendichi, F. Ossola, U. Russo, S. Simon, P. Tomasin and P. Vigato, *A. Polym Degrad Stab.*, **91**, (2006)3083

[3] D. Michoinova, "New Materials for the Protection of Cultural Heritage", Available at: http://www.arcchip.cz/w10/ w10_michoinova.pdf.

[4] J. T. Han, Y. Zheng, J. H. Cho, X. Xu and K. J. Cho., *Phys Chem. B,* **109**, (2005)20773

[5] R. P. J. Van Hees and H. J. P. Brocken, *Constr Build Mater*, **18,** (2004)331

[6] H. Teng, "Overview of the Development of the Fluoropolymer Industry", *Appl. Sci.*, **2,** (2012)496-512

[7] F. Estevão, B. Otavio , N. M. Johnny, E.C. M. Elisabeth and C. F. Maria Madalena, "Non-isothermal crystallization of PVDF/PMMA blends processed in low and high shear mixers", *Journal of Non-Crystalline Solids,* **358,** , (2012)2674–2681

[8] S. Jing , Y. Lu , Z. QiaoLing , H. Jin , S. Rui , M. Zhi , H. LingHao , H. Wei and H. Yong-Mei, "Modification on crystallization of poly(vinylidene fluoride) (PVDF) by solvent extraction of poly(methyl methacrylate) (PMMA) in PVDF/PMMA blends", *Frontiers of Materials Science,* 5, , (2011)388-400

[9] http: // www. Solvaysolexis. com/ pdf / Hylar 5000_ lg. pdf.

[10] http: // www. Plastics technology. com / articles / 2002 10 bib 1.html.

[11] B. L. Davis, J. E. Perry, D. C. Neth and K. C. Waters, J. *Applied Biomechanics*, **14,** , (1998)93-104

[12] R. Gregorio, S. Nociti, "Effect of PMMA addition on the solution crystallization of the α and β phase of poly(vinylidene fluoride)(PVDF)", *J. Phys. D: Appl. Phys.*, **28**, (1995) 432-436

[13] F. J. Lu and S. L. Hsu, *Macromolecules*, **19**, (1986) 326

[14] M. Suess, J. Kressler and H. W. Kammer, *Polymer*, **28**, (1987) 957

[15] R. Gregorio and M. Cestari, *Polymer Physics,* **32**, (1994)859-870

[16] M. Suess, J. Kressler and H. W. Kammer, Polymer, **28**, (1987) 957